Ciliopathy Protein Tmem107 Plays Multiple Roles in Craniofacial Development

P. Cela, M. Hampl, N.A. Shylo, K.J. Christopher, M. Kavkova, M. Landova, T. Zikmund, S.D. Weatherbee, J. Kaiser, and M. Buchtova

APPENDIX

APPENDIX METHODS

Generation of mice

The following information is provided by the MMRRC: Targeted or gene trap mutations are generated in strain 129/SvEvBrd-derived embryonic stem (ES) cells. The chimeric mice are bred to C57BL/6J albino mice to generate F1 heterozygous animals. These progeny are intercrossed to generate F2 wild type, heterozygous, and homozygous mutant progeny. On rare occasions, for example when very few F1 mice are obtained from the chimera, F1 heterozygous mice are crossed to 129/SvEvBrd x C57BL/6 hybrid mice to yield additional heterozygous animals for the intercross to generate the F2 mice. Mice are archived at the backcross generation N7.

Histological analysis

Samples were fixed in 4% buffered paraformaldehyde for at least overnight and then processed for histological analysis by a standard procedure (Behringer et al. 2014). Wild type, heterozygous and homozygous *Tmem107*$^{-/-}$ embryos were collected at stages E12.5 - E15.5 for microscopic analysis. Sections were photographed under bright-field illumination with a Leica compound microscope DMLB2 (Leica, Germany).

Immunohistochemical detection

Following deparaffinization and rehydration, antigen retrieval was carried out depending on the antibody host species (Appendix Table 2). Primary antibodies were applied for 1 hour at room temperature or overnight at 4°C. Secondary antibodies (goat anti-rabbit Alexa Fluor® 594, cat. No. A-11037; goat anti-mouse Alexa Fluor® 488, cat. No. A-11001; donkey anti-goat Alexa Fluor® 594 cat. No. A-11058, Thermo Fisher, USA) were applied for 30 minutes at room temperature. Sections were washed in PBS and coverslipped in Prolong Gold anti-fade reagent containing DAPI (cat. No. P36935, Invitrogen, USA) or stained with DRAQ5™ Fluorescent Probe Solution (cat. No. 62251, Thermo Fisher, USA) for confocal microscopy. The photos taken under a fluorescence microscope Leica DM LB2 (Leica Microsystems, Germany) were merged together in Adobe Photoshop 7.0 (USA). High power images were taken on confocal microscope Leica SP5 using 63x (oil) objectives (Leica Microsystems, Germany) with Leica Application Suite software.

For quantitative analysis of cell proliferation, PCNA-positive cells were counted in the area of palatal shelves. Mitotic index was calculated based on the ratio between number of proliferating cells and total number of cells. Three to five independent slides (with 4-6 sections) were analyzed for each stage of wt or *Tmem107*$^{-/-}$ mice.

TUNEL assay

Apoptotic cells were detected by a TUNEL assay (ApopTag Peroxidase in Situ Apoptosis Detection Kit, Cat. No. S7101, Chemicon, Temecula, USA). Nuclei were counterstained by Haematoxylin. The negative control was obtained by omitting the enzyme from the labelling protocol. Sections were photographed under bright-field illumination with a Leica compound microscope DMLB2 (Leica, Germany).

For quantitative analysis of cell apoptosis, TUNEL-positive cells were counted in the area of palatal shelves. Apoptotic index was calculated based on ratio between the number of apoptotic cells and total number of cells. Three independent slides (with 4-6 sections) were analyzed for each stage of wt or *Tmem107*$^{-/-}$ mice.

***In situ* hybridization**

In situ hybridizations were performed using standard methods (Behringer et al. 2014). The *Gli1* riboprobe plasmid (pBluescript) was a gift from Josh Catron. The *Shh* riboprobe plasmid (pBluescript II) was a gift from Andrew McMahon.

Statistical analysis

One-way ANOVA was used to assess statistical significance of measured values. Analyses were performed in Statistica 6.0 (StatSoft, Inc., Tulsa, USA). p-values were obtained using Bonferroni test. Differences between wt and *Tmem107*$^{-/-}$ were considered to be significant at $p < 0.05$. Level of significance is labelled as * $p < 0.05$, ** $p < 0.01$, *** $p < 0.001$.

Skeletal analysis

For skeleton analysis, embryonic heads were fixed in 100% ethanol and stained with Alcian Blue and Alizarin Red using standard methods (Behringer et al. 2014).

Skeleton on sections were stained by Alcian Blue and Sirius Red. Histological sections were rehydrated as described above. Samples were stained with 0.5% Alcian Blue (10 min), Haematoxylin (2 min), 2.5% Phosphomolybden Acid (10 min) and 0.1% Sirius Red (1 h).

Scanning electron microscopy (SEM)

Embryos were fixed in 4% paraformaldehyde, washed in distilled water and dehydrated through a graded series (30-100%) of ethanol solutions. Then, samples were dried out using CPD 030 Critical Point Dryer (BAL-TEC) and shadowed by gold in metal shadowing apparatus Balzers SCD040. Samples were observed and photographed in the scanning electron microscope TESCAN Vega TS 5136 XM (Tescan, Czech Republic).

Micro-computed tomography analysis

MicroCT analysis was performed by on E15.5 *Tmem107*$^{-/-}$ embryos and wt as controls. Each embryo was scanned twice. The first measurement was performed without any sample staining to visualize only the ossified tissue. For the second measurement, the samples were stained by Phosphotungstic Acid (PTA) to enhance contrast of soft tissue (Metscher 2009).

The microCT meausurement was performed using the GE Phoenix v|tome|x L 240 laboratory system equipped with 180 kV / 15 W nanofocus tube. The measurements were carried out at acceleration voltage of 60 kV and X-ray tube current of 200 µA. The acquisition time was 900 ms in every 2000 images of the 360° rotation. The microCT data were obtained with voxel resolution of 4.5 µm.

The tomographic reconstruction was realized by GE phoenix datos|x 2.0 software. The manual segmentation of microCT data and 3D model imaging were implemented in VG Studio software MAX.

APPENDIX REFERENCES

Behringer R, Gertsenstein M, Vinterstein Nagy K, Nagy A. 2014. Manipulating the mouse embryo: A laboratory manual. New York: Cold Spring Harbor Laboratory Press.

Metscher BD. 2009. MicroCT for comparative morphology: simple staining methods allow high-contrast 3D imaging of diverse non-mineralized animal tissues. BMC Physiol 9:1-11.

APPENDIX FIGURES

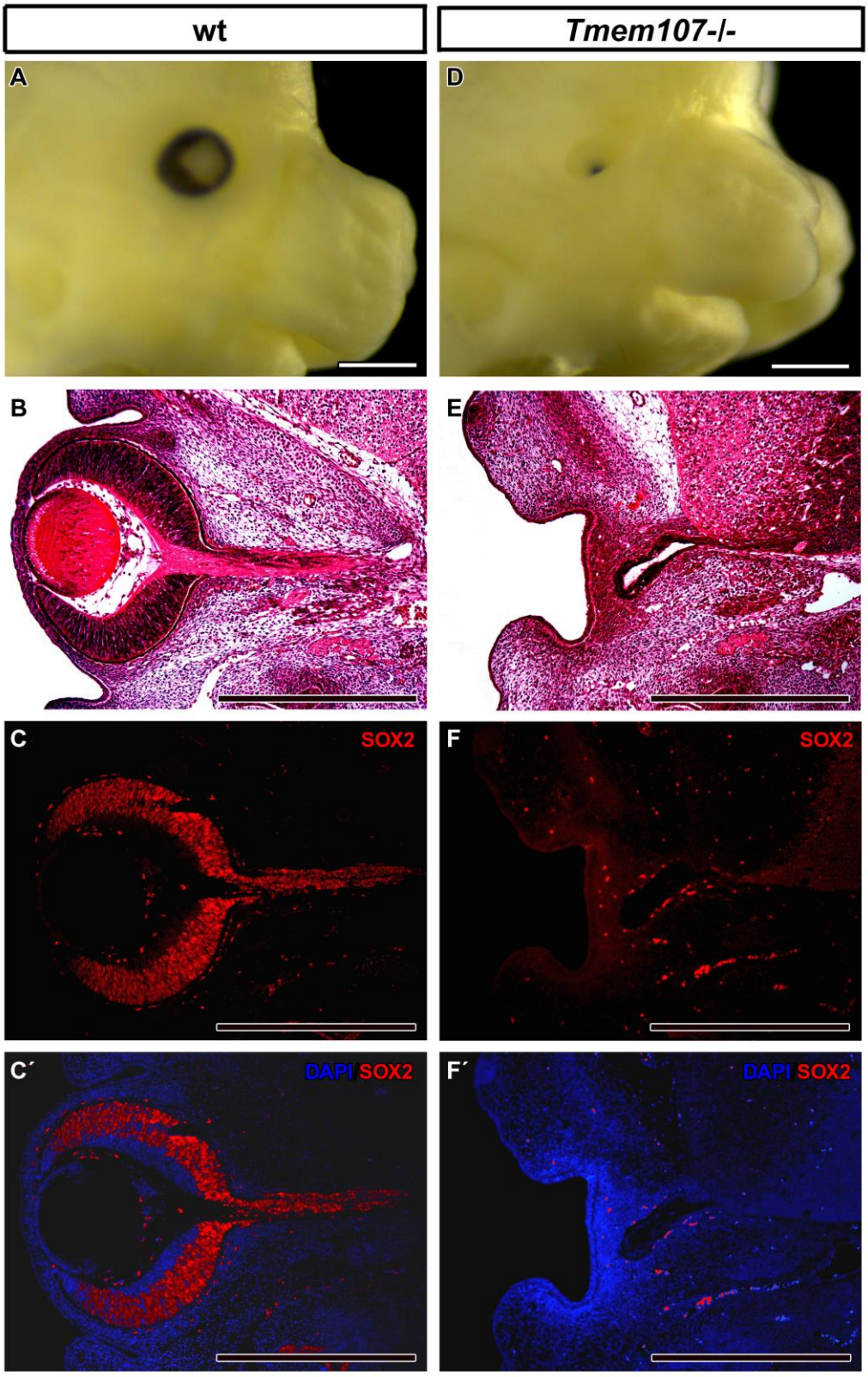

Appendix Figure 1: **Eye phenotype in *Tmem107*$^{-/-}$ mouse at stage E13.5**

External view of wt eye (A). Frontal section of normal developing eye (B). SOX2 expression in retina and nervus opticus of eye in wt animals (C, C´). External view of *Tmem107*$^{-/-}$ mouse eye (D). Frontal section of eye rudiment, where only ectodermal sack and retinal rudiment have developed (E). There is no SOX2 expression in eye of *Tmem107*$^{-/-}$ mouse (F, F´). Scale bars = 500 µm.

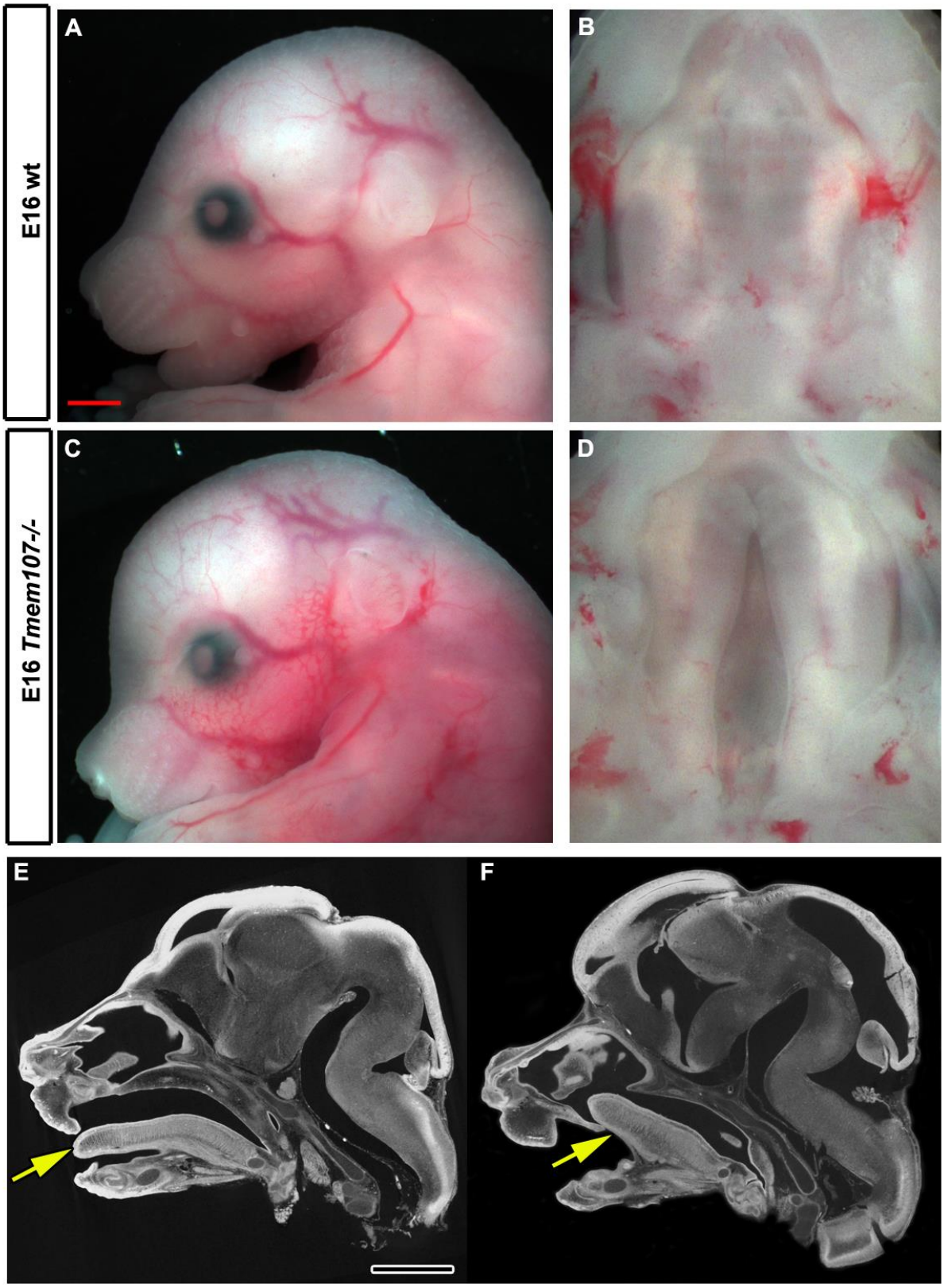

Appendix Figure 2: External head phenotype and palatal cleft

Lateral view of wild type (A) and mutant embryo (C) of stage E16 mouse. Extensive cleft palate is visible in *Tmem107*$^{-/-}$ embryo (D) in comparison to physiologically developed palate of wild type animal (B). Sagittal sections of wt (E) and *Tmem107*$^{-/-}$ E15.5 embryos (F) scanned in MicroCT. Embryos were labelled in PTA to visualize soft tissues. Note the tongue position and its size in *Tmem107*$^{-/-}$ mice. Scale bar = 1 mm.

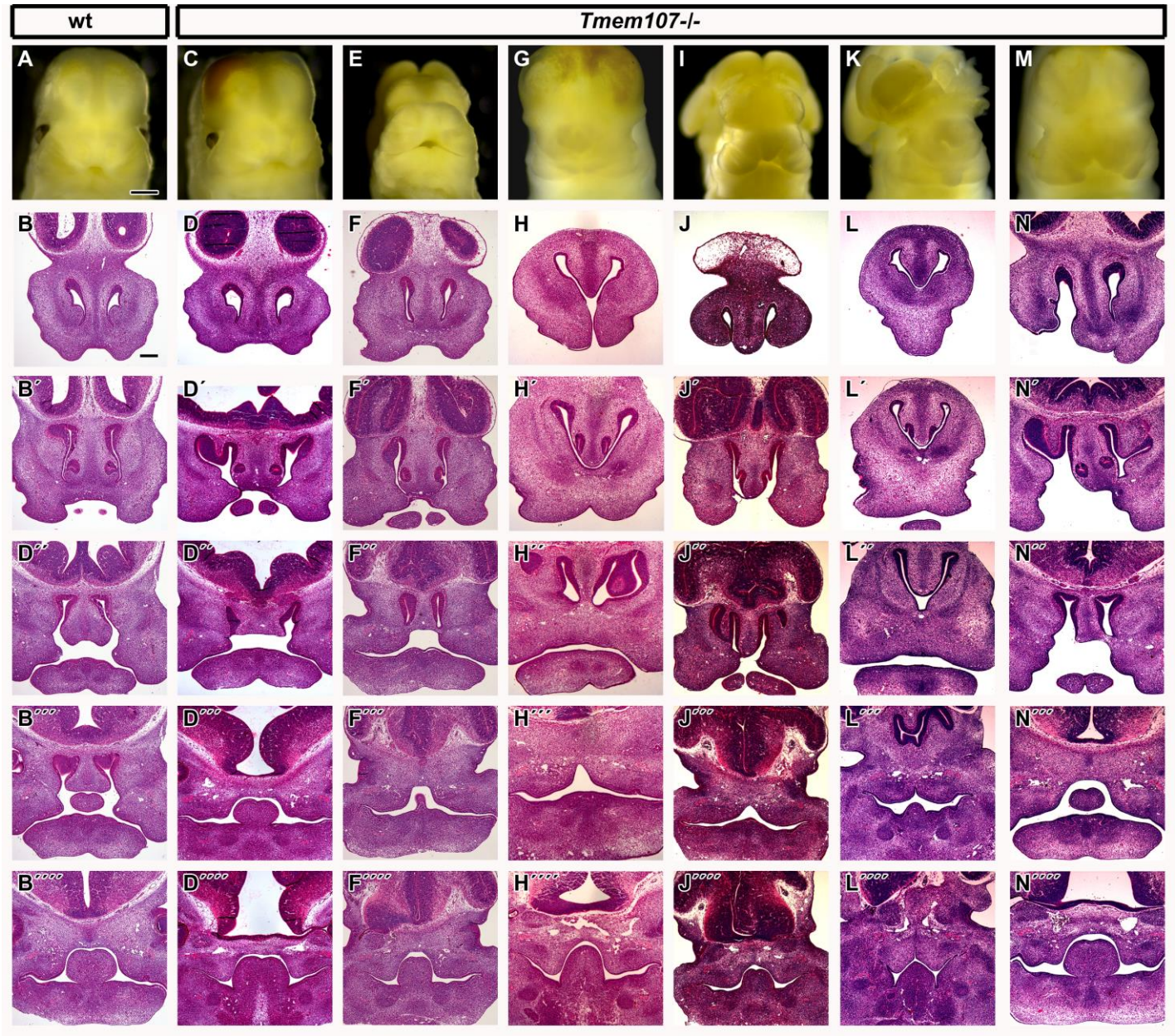

Appendix Figure 3: External phenotypes and frontal sections of face in rostro-caudal direction at stage E12.5

External view of wt embryo head (A). Externally *Tmem107*$^{-/-}$ mice exhibit various degrees of phenotypic changes including exencephalia, anophthalmia and cleft lip (C, E, G, I, K, M). Frontal section of littermate control (A) with normally developed palatal processes and other facial structures (B-B´´´´). Frontal sections of *Tmem107*$^{-/-}$ mouse (C) with shorter and thicker nasal septum and smaller palatal processes (D-D´´´´). Frontal sections of *Tmem107*$^{-/-}$ mouse (E) with defects in development of nasal septum, nasal and oral cavities and small tongue (F-F´´´´). Frontal sections of *Tmem107*$^{-/-}$ mouse (G) with rudimental nasal and oral cavity and reduced palatal processes (H-H´´´´). Frontal sections of *Tmem107*$^{-/-}$ mouse (I) with reduced nasal septum, oral cavity, tongue and palatal processes (J-J´´´´). Frontal sections of *Tmem107*$^{-/-}$ mouse (K), with no connection between nasal and oral cavity; also there is reduced nasal septum, tongue and almost no obvious palatal processes (L-L´´´´). Frontal sections of *Tmem107*$^{-/-}$ mouse (M) with distinct cleft in the rostral part of the jaw and deformed nasal septum (N-N´´´´). All embryos exhibit various defects in brain morphology. Scale bars = 500 µm for external images and 200 µm for histological sections.

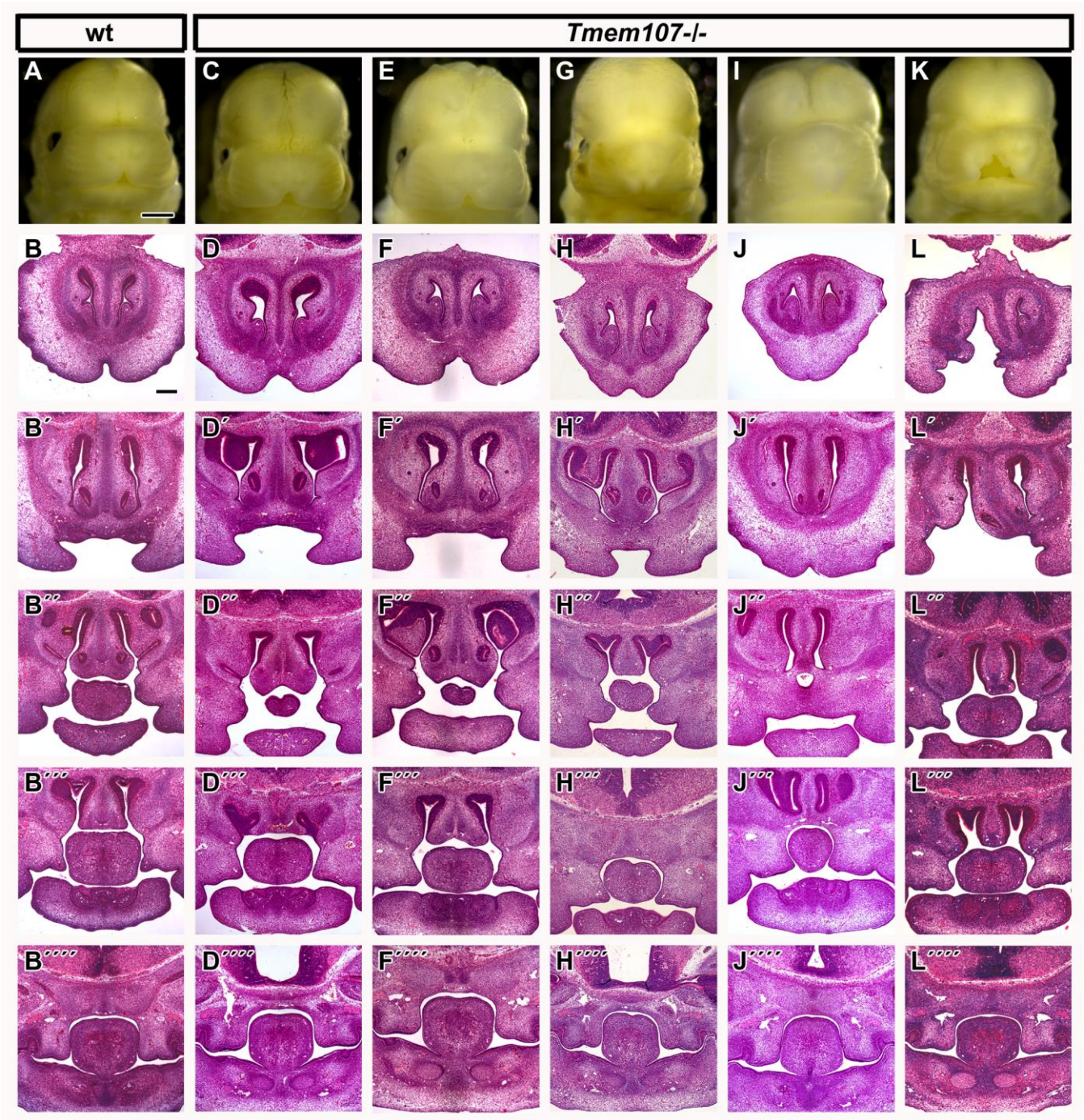

Appendix Figure 4: External phenotypes and frontal sections of face in rostro-caudal direction at stage E13.5

External view of wt embryo head (A). Externally, *Tmem107*$^{-/-}$ embryos display various degree of phenotypical changes, including snout defects, anophthalmia and cleft lip (C, E, G, I, K). Frontal section of wt mouse (A) with normally developed palatal processes and other facial structures (B-B´´´´). Frontal sections of *Tmem107*$^{-/-}$ mouse (C) exhibit expanded midline (D-D´´´´). Frontal sections of *Tmem107*$^{-/-}$ mouse (E) also demonstrate expanded midline structures (F-F´´´´). Frontal sections of *Tmem107*$^{-/-}$ mouse (G) with narrow snout, reduced nasal septum and palatal processes improperly oriented below the tongue (H-H´´´´). Frontal sections of *Tmem107*$^{-/-}$ mouse (I) with narrow nasal septum and abnormal palatal processes oriented below the tongue (J-J´´´´). Frontal sections of *Tmem107*$^{-/-}$ mouse (K) with distinct cleft lip and deformed nasal septum, however palatal processes are developed normally (L-L´´´´). Scale bars = 500 µm for external images and 200 µm for histological sections.

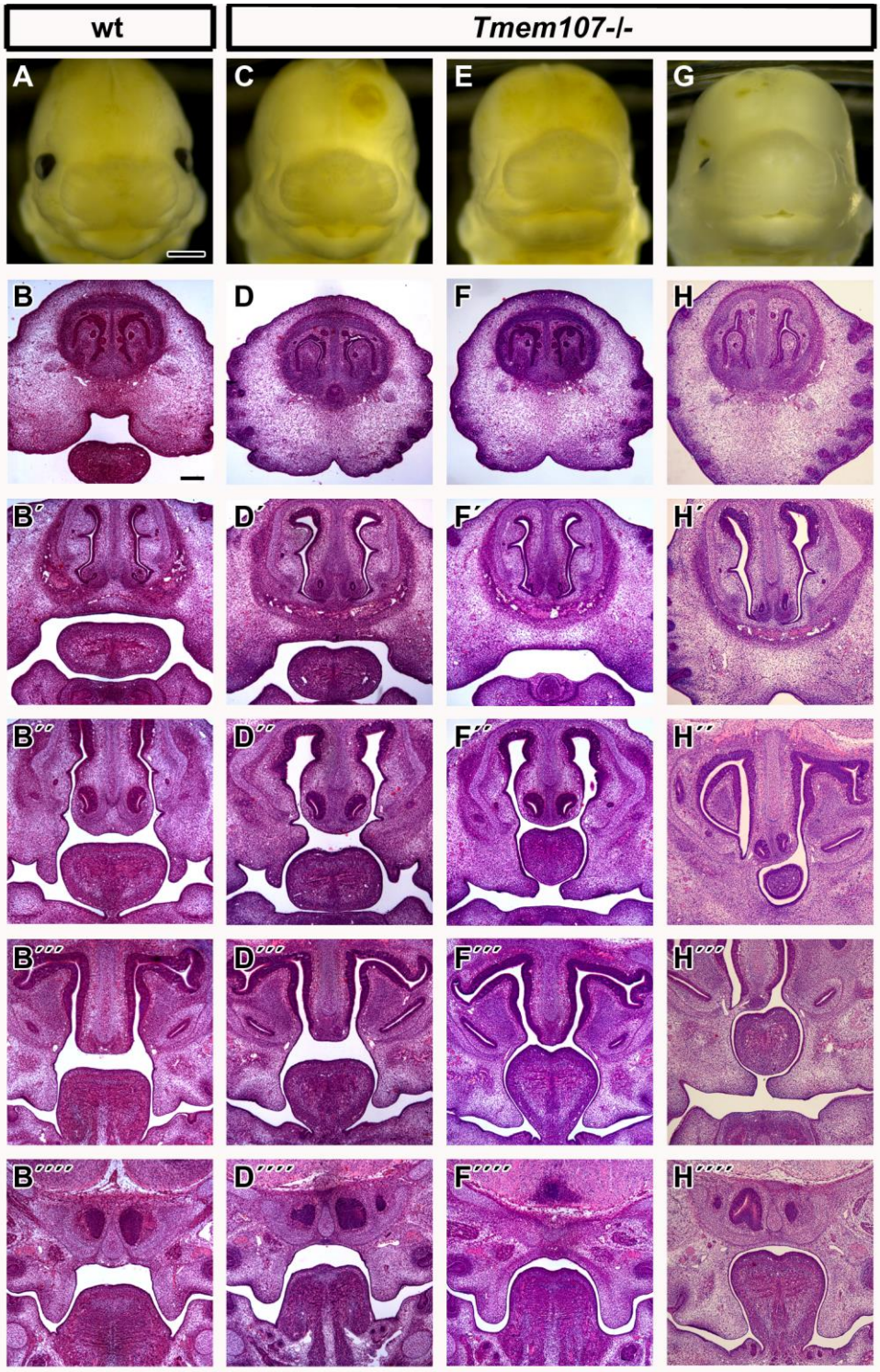

Appendix Figure 5: External phenotypes and frontal sections of face in rostro-caudal direction at stage E14.5

External view of wt embryo head (A). Externally, *Tmem107*$^{-/-}$ embryos display microophthalmia or anophthalmia and slightly atypical snout (C, E, G). Frontal section of wt mouse (A) with normally developed palatal processes and other facial structures (B-B´´´´). Frontal sections of *Tmem107*$^{-/-}$ mouse (C) exhibit slightly shorter palatal septum and broader nasal cavities (D-D´´´´). Frontal sections of *Tmem107*$^{-/-}$ mouse (E) with defects in nasal septum, thicker palatal shelves improperly oriented below the tongue (F-F´´´´). Frontal sections of *Tmem107*$^{-/-}$ mouse (G) with the most affected animal at stage E14.5, narrow and deformed nasal septum and thick palatal shelves oriented below the tongue (H-H´´´´). Scale bars = 500 µm for external images and 200 µm for histological sections.

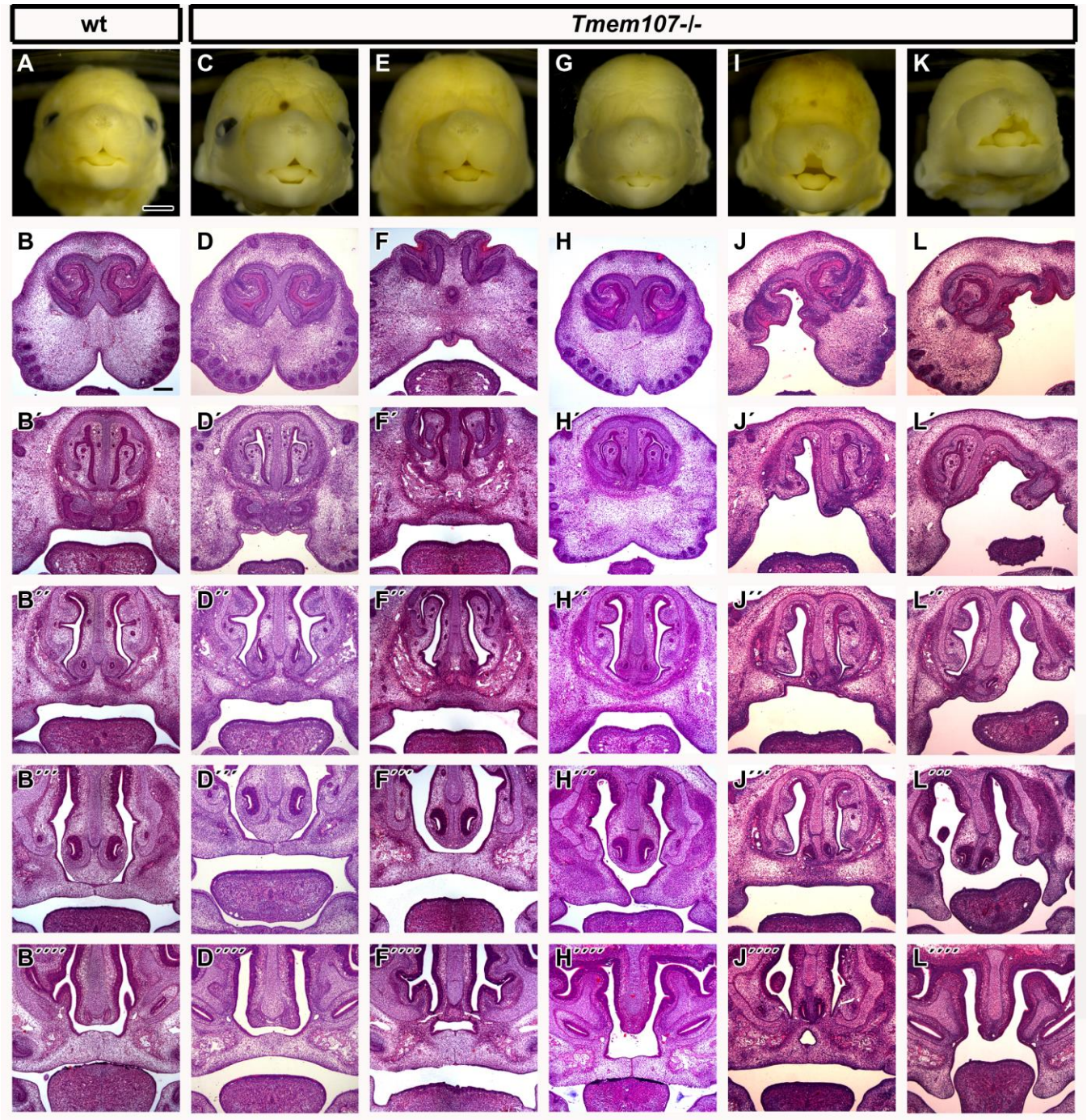

Appendix Figure 6: External phenotypes and frontal sections of face in rostro-caudal direction at stage E15.5

External view of wt embryo head (A). Externally, *Tmem107*$^{-/-}$ embryos exhibit anophthalmia and massive cleft lip (C, E, G, I, K). Frontal section of wt mouse (A) with normally developed palatal processes, which fused together in horizontal position (B-B´´´´). Frontal sections of *Tmem107*$^{-/-}$ mouse (C) with only mild phenotype (D-D´´´´). Frontal sections of *Tmem107*$^{-/-}$ mouse (E) are slightly obliged, nasal septum is shorter and thinner (F-F´´´´). Frontal sections of *Tmem107*$^{-/-}$ mouse (G) with the cleft of secondary palate and no fused palatal processes in the anterior palatal area (H-H´´´´). Frontal sections of *Tmem107*$^{-/-}$ mouse (I) with prominent one-side cleft and deformed nasal septum (J-J´´´´). Frontal sections of *Tmem107*$^{-/-}$ mouse (K) with the most affected animal of this stage (L-L´´´´). There is a prominent one-side complete cleft, deformed nasal septum and palatal processes improperly oriented below the tongue. Scale bars = 500 µm for external images and 200 µm for histological sections.

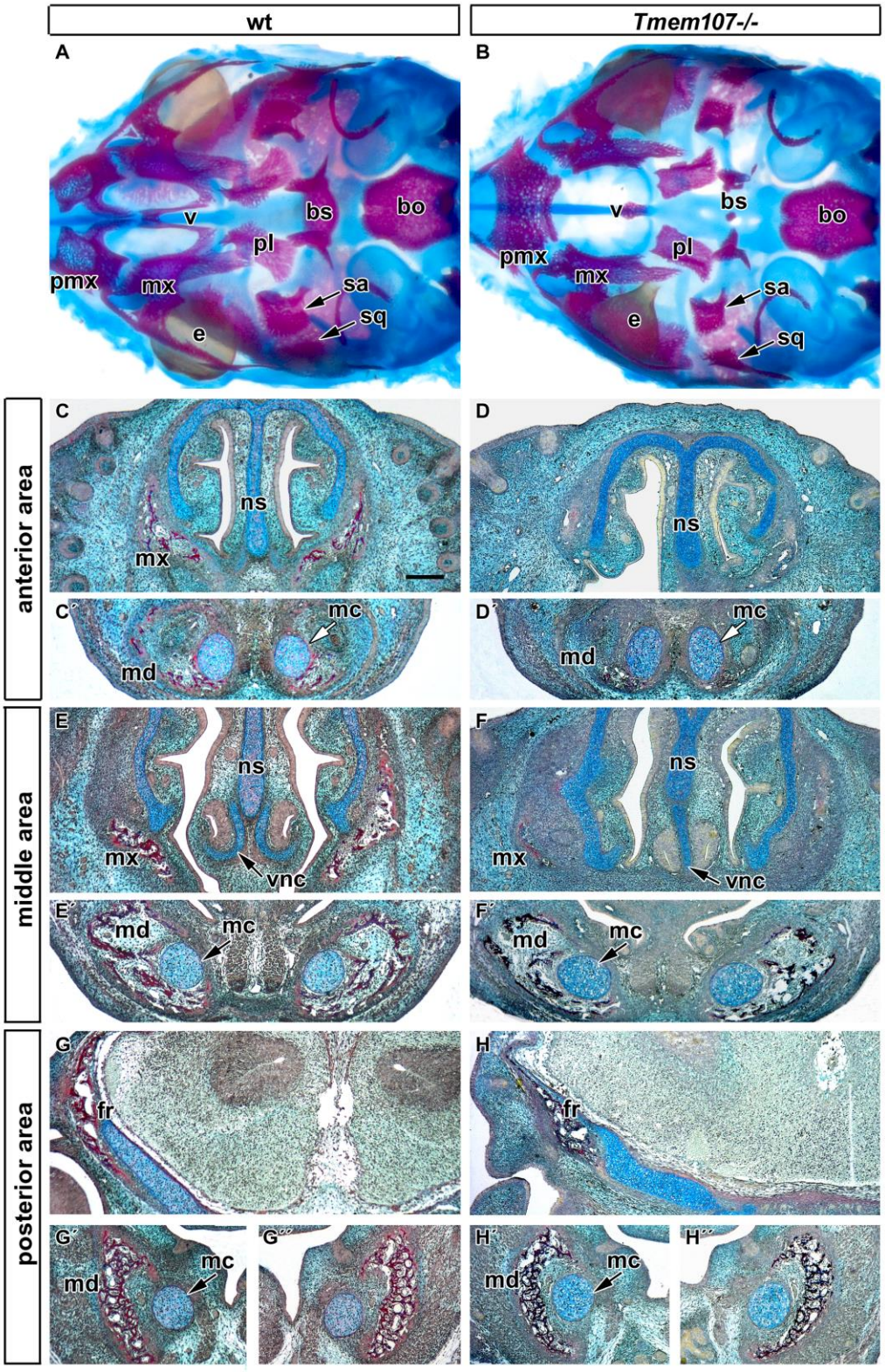

Appendix Figure 7: Intramembranous bone ossification in *Tmem107*$^{-/-}$ mice

Detailed view of Alcian Blue/Alizarin Red staining at E16.5 demonstrates altered morphology of vomer (v), basisphenoid (bs), sphenoid ala (sa), palatine (pl), premaxillary (pmx) and maxillary (mx) bones, pars squamosa ossis temporalis (sq) in *Tmem107*$^{-/-}$ embryos (B) in comparison to wt (A). Moreover, eye (e) size and shape is altered in *Tmem107*$^{-/-}$ mice (B). Frontal sections of the wt (C, E, G) and *Tmem107*$^{-/-}$ embryo (D, F, H) of stage E15.5 in rostro-caudal direction stained with Alcian Blue and Sirius Red. Delayed mineralization (red colour) and shape differences are shown in maxillary (mx), mandibular (md) and frontal (fr) bones in *Tmem107*$^{-/-}$ mouse. Moreover, shape of Meckel´s cartilage (mc) and vomeronasal cartilage (vnc) is altered. Nasal septum (ns) is slightly wider in *Tmem107*$^{-/-}$ embryos. bo – basioccipital bone. Scale bar = 100 µm.

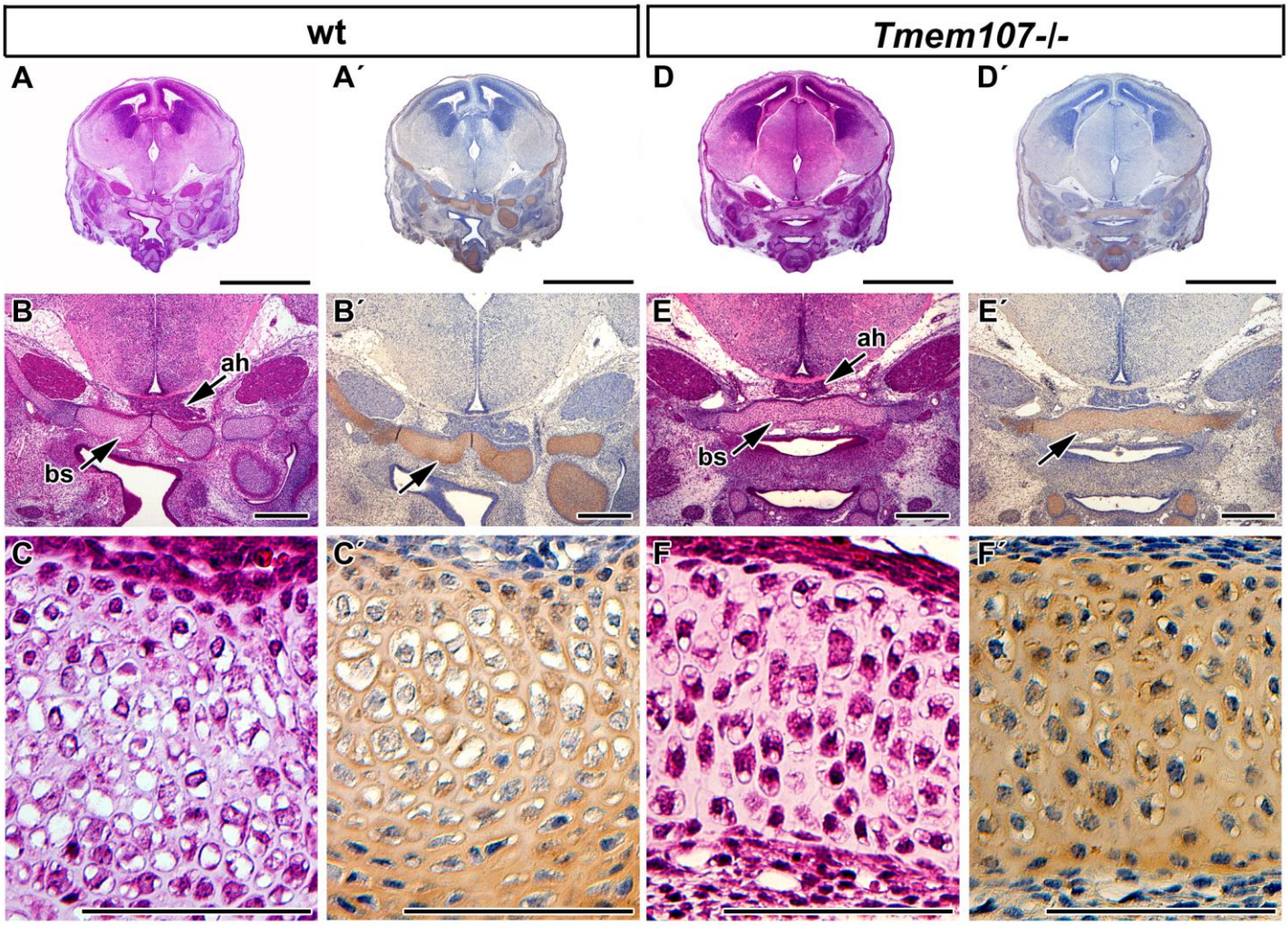

Appendix Figure 8: Chondrogenesis in *Tmem107*$^{-/-}$ mice

Frontal sections in the area of basisphenoid cartilage (bs) and adenohypophysis (ah) in wt (A, A´) and *Tmem107*$^{-/-}$ embryos at E15.5 (D, D´). Expression of Collagen 2 in the basisphenoid cartilage (A´, E´) and alternative sections stained by Haematoxylin (B, E). Detailed views demonstrate advanced development of chondrogenesis in basoisphenoid cartilage with hypertrophic cartilage in wt (C, C´) in comparison to delayed development in *Tmem107*$^{-/-}$ animals (F, F´).

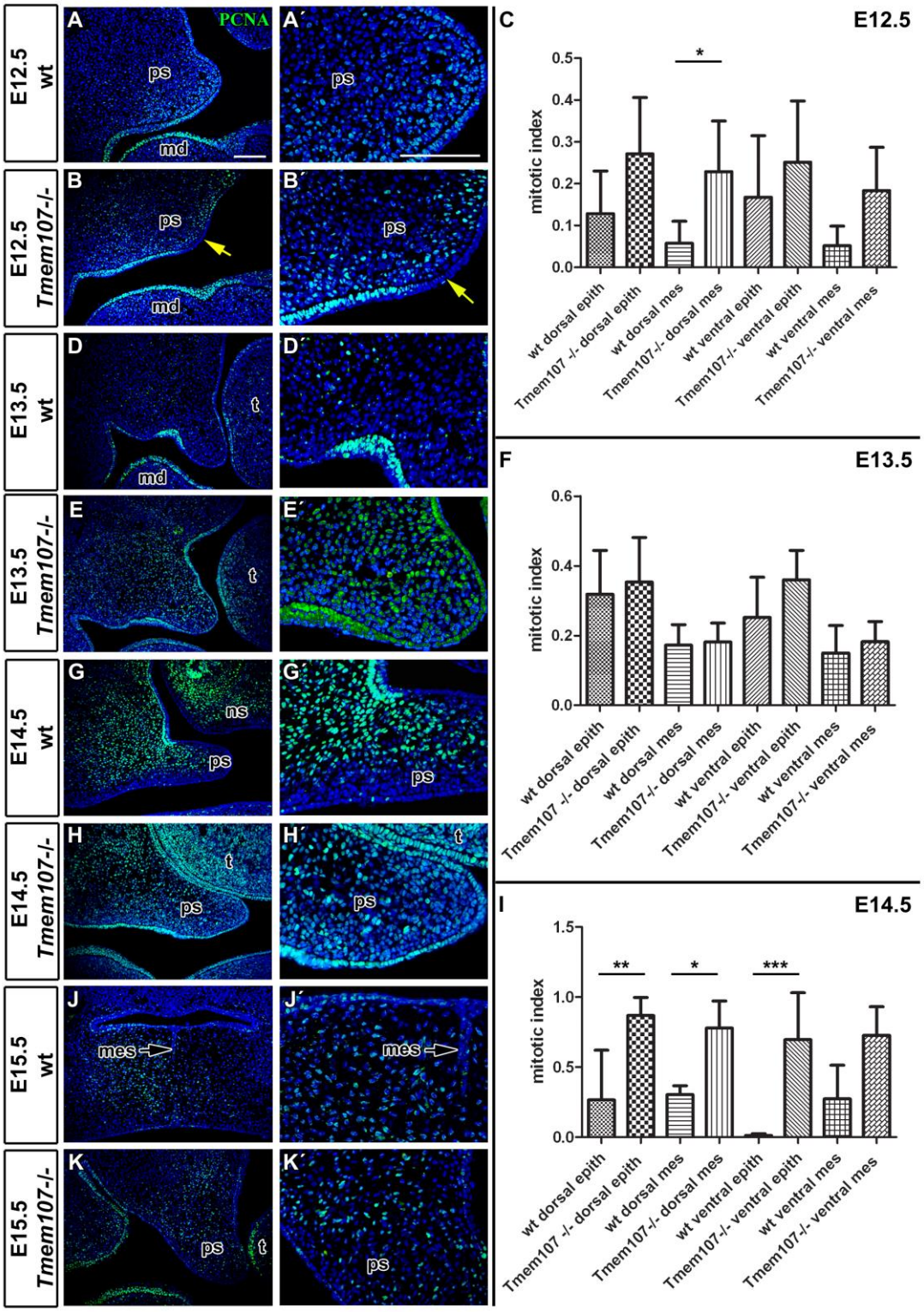

Appendix Figure 9: Detection of proliferating cells in the palatal shelves of *Tmem107*$^{-/-}$ animals

Proliferating cells were visualized by immunofluorescent labeling for PCNA, where positive cells are labeled by Alexa 488 (green) (A-K). We observed lower number of PCNA-positive cells in the mesenchyme of wt (A, D, G, J) in comparison to *Tmem107*$^{-/-}$ mutants (B, E, H, K). Upregulated proliferation is detected also in the palatal epithelium. Low level of proliferation was observed at E15.5 both in *Tmem107*$^{-/-}$ (K, K´) and wt mice (J, J´). Mitotic index (C, F, I) was counted as the ratio between PCNA-positive cells and total amount of cells in the palatal shelves with statistically significant differences found only in dorsal mesenchyme of E12.5 (C) and most of the analyzed areas at E14.5 (I). The graphs values denote average ± s.d., * $p < 0.05$, ** $p < 0.01$, *** $p < 0.001$ by one-way ANOVA. Nuclei are counterstained by DAPI (blue). md – mandible, ns – nasal septum, ps - palatal shelf, mes – medial epithelial seam, t -tongue. Scale bars = 100 µm.

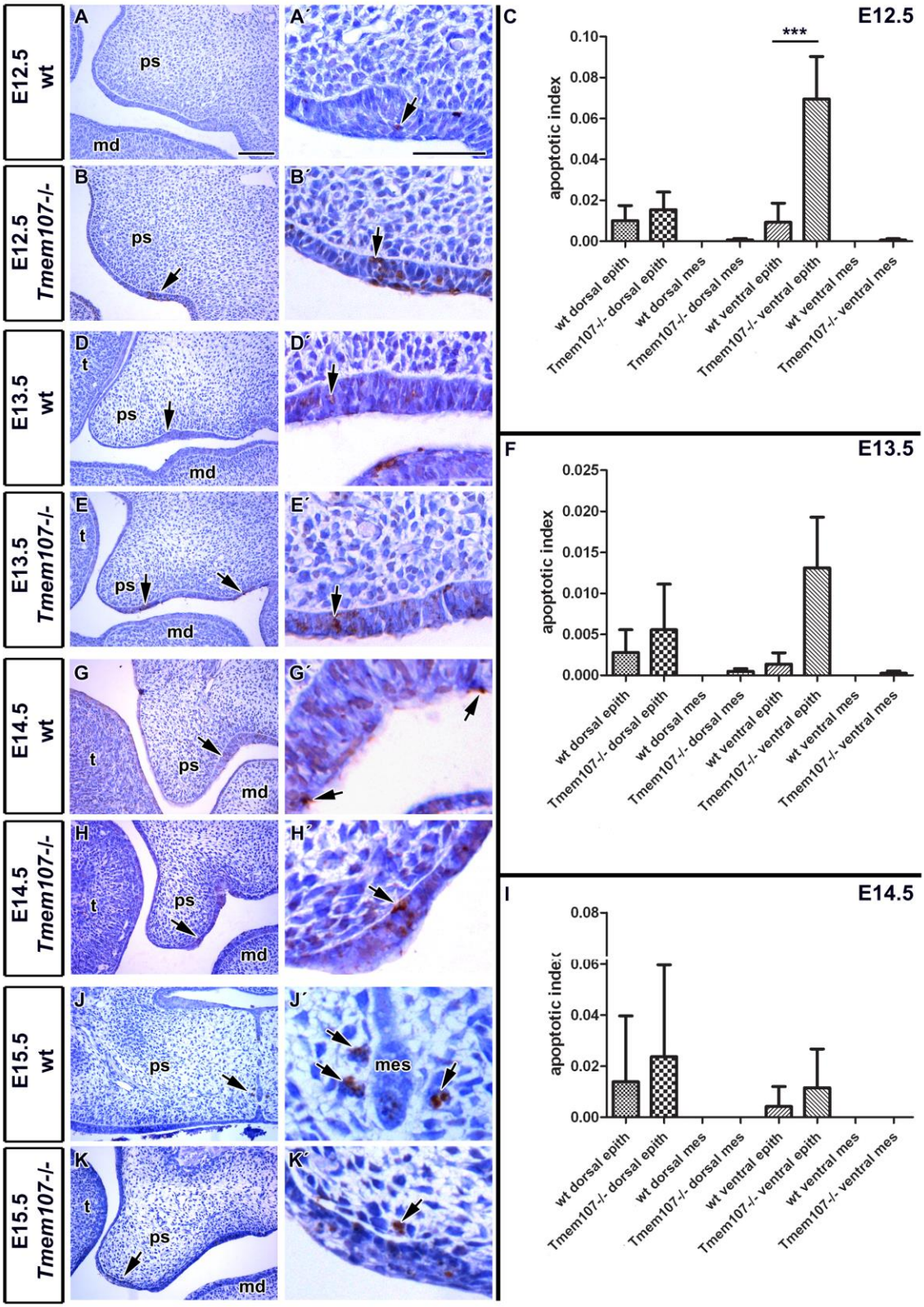

Appendix Figure 10: Detection of apoptotic cells in the palatal shelves of *Tmem107*$^{-/-}$ animals

There are only few apoptotic cells (brown) in wt animals (A, D, G, J) with a higher presence only at E15.5 around the palatal seam area (J, J´). Several TUNEL-positive cells (arrow) are located in the ventral epithelium of palatal shelves in *Tmem107*$^{-/-}$ mice (B, E, H, K) and in the tip of the palatal shelves at E15.5 (K, K´). Nuclei are counterstained by Haematoxylin. TUNEL-positive areas are labeled by arrows. The graphs values denote average ± s.d. *** $p < 0.001$ by one-way ANOVA. md – mandible, ps – palatal shelf, mes – medial epithelial seam, t – tongue. Scale bars of lower magnification = 100 µm, scale bars of higher magnification = 50 µm.

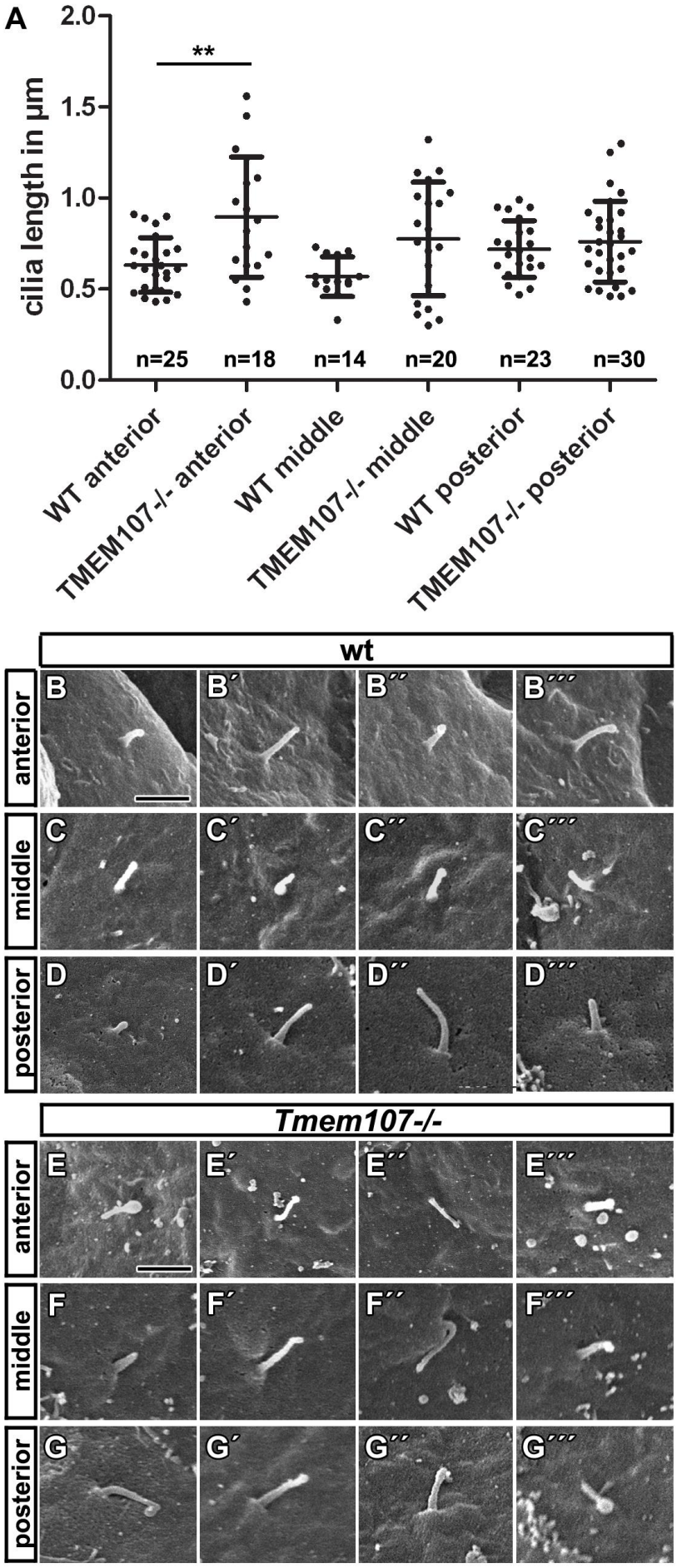

Appendix Figure 11: Variability in cilia length and morphology on the epithelium of palatal shelves

Graph represents summary of differences in cilia length between all three analyzed areas (A). Relevant statistically significant differences are highlighted. Sample size for individual treatments is indicated (n) and the graph values denote distribution of individual measurements ± s.d., where ** $p < 0.01$ by one-way ANOVA.

High magnification of epithelial primary cilia in the anterior, middle and posterior areas of the palatal shelves. Altered length and morphology of primary cilia is observed in *Tmem107*$^{-/-}$ mutants (E-G´´´´) compared to controls (B-D´´´´). Numerous elongated cilia or cilia with bulges on their tips were detected. Scale bar = 1 µm.

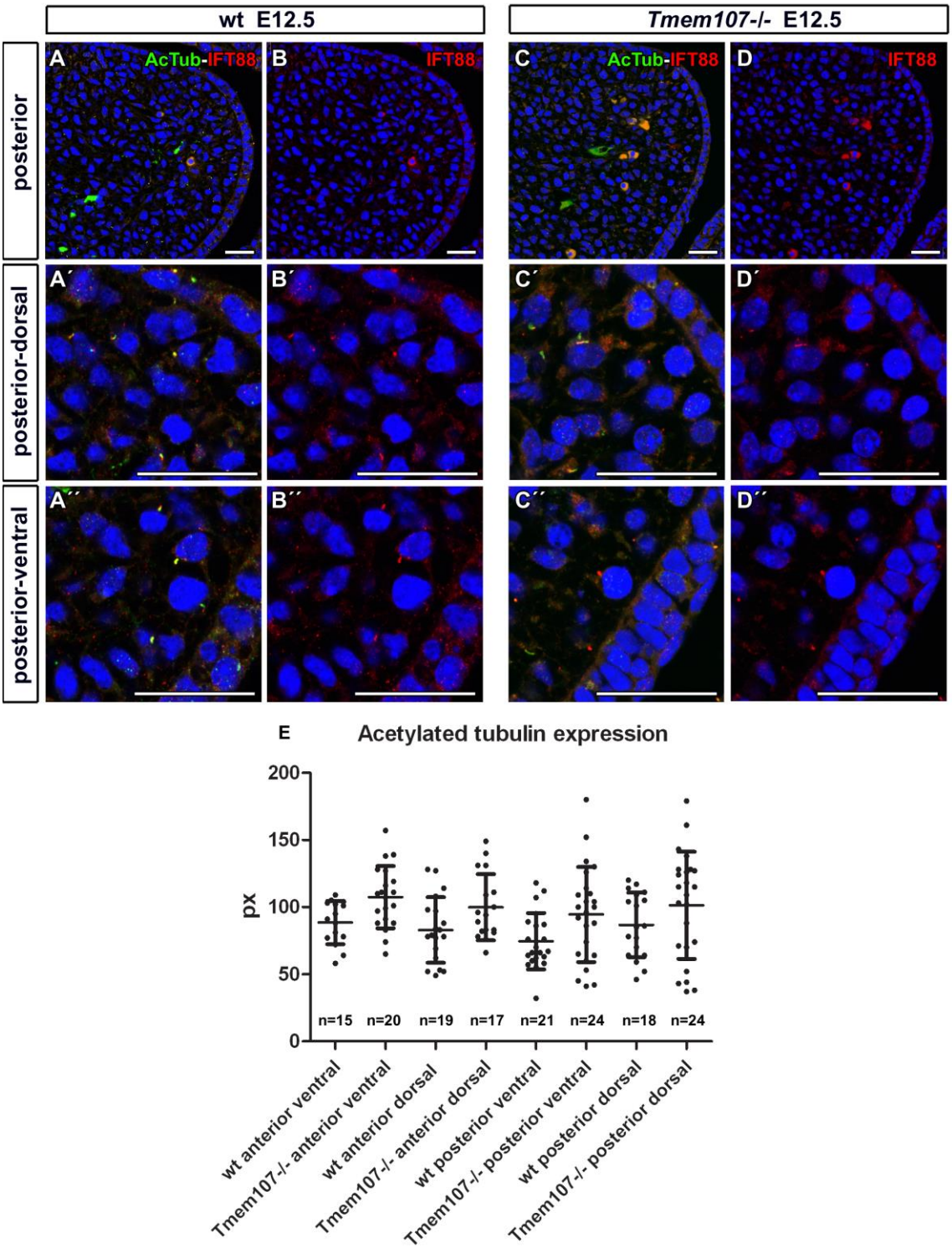

Appendix Figure 12: IFT88 expression in the posterior area of palatal shelves in *Tmem107*$^{-/-}$ animals at E12.5

Double labeling for acetylated alpha-tubulin (green) and IFT88 (red) in developing palatal shelves of wt (A-A´´, B-B´´) and *Tmem107*$^{-/-}$ (C-C´´, D-D´´) mice. In the posterior area, cilia appear to be longer in the dorsal part of palatal shelves of *Tmem107*$^{-/-}$ mouse (C´, D´), in contrast to wt (A´, B´). In the ventral area of posterior shelves, the difference in acetylated alpha-tubulin and IFT88 expression is not so clearly visible in contrast to dorsal areas between *Tmem107*$^{-/-}$ mouse (C´´, D´´) and WT mouse (A´´, B´´). Scale bar = 25 µm.

Graph represents summary of differences in acetylated alpha-tubulin expression in mesenchymal cilia between all three analyzed areas (E). We have not found any significant statistical differences between wt and *Tmem107*$^{-/-}$ by one-way ANOVA. Sample size for individual treatments is indicated (n), the graph values denote distribution of individual measurements. px – pixels of expression.

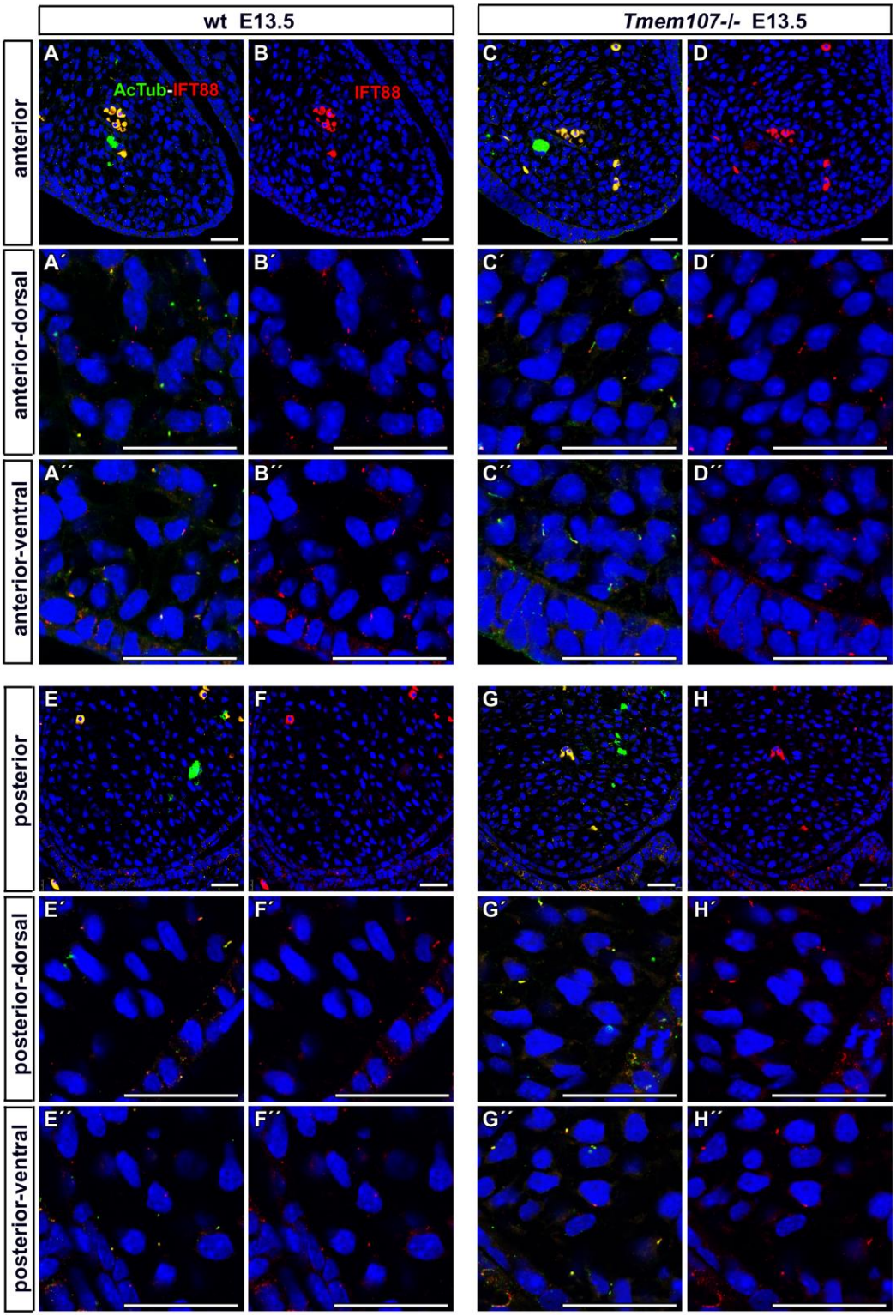

Appendix Figure 13: IFT88 expression in the palatal shelves in *Tmem107*$^{-/-}$ animals at E13.5

Double labeling for acetylated alpha-tubulin (green) and IFT88 (red) in developing palatal shelves of wt (A-A´´, B-B´´) and *Tmem107*$^{-/-}$ (C-C´´, D-D´´) mice at E13.5. Primary cilia labeled by acetylated alpha-tubulin appear to be longer and have altered shape in *Tmem107*$^{-/-}$ (C´, C´´, D´, D´´) in comparison to wt mice (A´, A´´, B´, B´´) in both analyzed areas of the anterior palatal shelves. IFT88 expression is upregulated in several cilia of *Tmem107*$^{-/-}$ mice (D´) in comparison to wt animals (B´). In the posterior area, cilia are clearly longer in the dorsal part of palatal shelves of *Tmem107*$^{-/-}$ mouse (G-G´´, H-H´´) in contrast to wt animals (E-E´´, F-F´´). In the ventral area of posterior shelves, the difference in alpha-acetylated tubulin and IFT88 expression patterns is less visible in contrast to dorsal areas between *Tmem107*$^{-/-}$ mouse (G´´, H´´) and wt mouse (E´´, F´´). Scale bar = 25 μm.

APPENDIX MOVIES

Appendix Movie 1: Ossification centers of E15.5 wt animal visualized by microCT

Appendix Movie 2: Ossification centers of E15.5 *Tmem107*$^{-/-}$ animal visualized by microCT

Appendix Table 1: Analysis of most prominent external phenotypes in all analyzed stages

E12.5	EXENCEPHALY	MICROOPHTHALMY	ANOPHTHALMY	CLEFT LIP	DEFORMED SNOUT
wt (n=8)	0	0	0	0	0
Tmem107$^{+/-}$ (n=5)	0	0	0	0	0
Tmem107$^{-/-}$ (n=10)	3	2	5	1	4
E13.5					
wt (n=8)	0	0	0	0	0
Tmem107$^{+/-}$ (n=10)	0	0	1	0	0
Tmem107$^{-/-}$ (n=14)	0	2	3	2	3
E14.5					
wt (n=8)	0	0	0	0	0
Tmem107$^{+/-}$ (n=4)	0	0	0	0	0
Tmem107$^{-/-}$ (n=9)	1	2	5	1	2
E15.5					
wt (n=9)	0	0	0	0	0
Tmem107$^{+/-}$ (n=13)	0	0	0	0	0
Tmem107$^{-/-}$ (n=9)	0	1	7	3	2

Appendix Table 2: List of primary antibodies used for immunolabelling

Antibody	**Type of antibody**	**Company, catalogue number**	**Pretreatment**	**Dilution of primary antibody**
Sox2	Rabbit-polyclonal	Cell Signaling Technologies, 2748S	0,25% Trypsin/37 ºC; Target Retrieval Solution, pH 9, DAKO, cat.n. S2367, 15 min/97 ºC in water bath	1:100
Sox9	Rabbit-polyclonal	Sigma Aldrich, HPA001758	Citrate buffer, pH6, 10mM, 20 min/97 ºC in water bath	1:200
Acetylated alpha tubulin	Mouse-monoclonal	Life Technologies, 32-2700	Target Retrieval Solution, pH 9, DAKO, cat.n. S2367, 20 min/97 ºC in water bath	1:200
IFT88	Goat-polyclonal	Sigma Aldrich, SAB2500530	Target Retrieval Solution, pH 9, DAKO, cat.n. S2367, 20 min/97 ºC in water bath	1:200
PCNA	Mouse-monoclonal	DAKO, M0879	Citrate buffer, pH6, 10mM, 25 min/97 ºC in water bath	1:50
Col2	Rabbit-polyclonal	Abcam, ab53047	Citrate buffer, pH6, 10mM, 30 min/97 ºC in water bath	1:100